nature geoscience

Article

https://doi.org/10.1038/s41561-024-01393-6

Global emergent responses of stream microbial metabolism to glacier shrinkage

Received: 31 May 2023

Accepted: 30 January 2024

Published online: 1 March 2024

Check for updates

Tyler J. Kohler[1,2] ✉, Massimo Bourquin[1], Hannes Peter[1], Gabriel Yvon-Durocher[3], Robert L. Sinsabaugh[4], Nicola Deluigi[1], Michael Styllas[1], Vanishing Glaciers Field Team* & Tom J. Battin[1] ✉

Most cryospheric ecosystems are energy limited. How their energetics will respond to climate change remains largely unknown. This is particularly true for glacier-fed streams, which interface with the cryosphere and initiate some of Earth's largest river systems. Here, by studying resource stoichiometry and microbial energetics in 154 glacier-fed streams sampled by the Vanishing Glaciers project across Earth's major mountain ranges, we show that these ecosystems and their benthic microbiome are overall carbon and phosphorus limited. Threshold elemental ratios and low carbon use efficiencies (median: 0.15) modelled from extracellular enzymatic activities corroborate resource limitation in agreement with maintenance metabolism of benthic microorganisms. Space-for-time substitution analyses suggest that glacier shrinkage will stimulate benthic primary production in glacier-fed streams, thereby relieving microbial metabolism from carbon limitation. Concomitantly, we find that increasing streamwater temperature will probably stimulate microbial growth (temperature sensitivity: 0.62 eV). Consequently, elevated microbial demands for phosphorus, but diminishing inputs from subglacial sources, may intensify phosphorus limitation as glaciers shrink. Our study thus unveils a 'green transition' towards autotrophy in the world's glacier-fed streams, entailing shifts in the energetics of their microorganisms.

Fluvial ecosystems are among the most heterotrophic ecosystems on Earth and are major emitters of CO_2 to the atmosphere[1,2]. The notion of stream and river heterotrophy has its root in studies of ecosystems draining forested catchments, where terrestrial subsidies of organic carbon (C) are commonplace[3,4]. In these ecosystems, microorganisms degrade allochthonous organic C and are rarely limited by C but rather by nitrogen (N) and phosphorus (P)[5]. Conversely, streams that drain catchments with poorly developed terrestrial vegetation—characteristic of high-altitude, high-latitude and arid biomes—do not fit this model, and their microbial metabolism can be C limited[6]. Understanding the mechanisms underpinning microbial energetics in fluvial ecosystems is critical because it potentially links to the global C cycle[2].

The microbial metabolism of glacier-fed streams (GFSs) that drain the world's major mountain ranges may be particularly C limited. Near glaciers, GFSs drain largely mineral terrain devoid of terrestrial production and developed soils. Glaciers deliver bio-reactive dissolved organic carbon (DOC) to the downstream microbial metabolism, albeit at low concentrations[7,8]. Furthermore, autochthonous production in GFSs is low because of physical disturbances and light-attenuating turbidity induced by unconsolidated sediments and turbulent flow[9,10]. Because

[1]River Ecosystems Laboratory, Alpine and Polar Environmental Research Center, Ecole Polytechnique Fédérale de Lausanne (EPFL), Sion, Switzerland. [2]Department of Ecology, Faculty of Science, Charles University, Prague, Czechia. [3]Environment and Sustainability Institute, University of Exeter, Exeter, UK. [4]Department of Biology, University of New Mexico, Albuquerque, NM, USA. *A list of authors and their affiliations appears at the end of the paper. ✉e-mail: tyler.j.kohler@gmail.com; tom.battin@epfl.ch

of the scarcity of organic C sources, GFS metabolism is often sustained by chemolithotrophy (for example, sulfur, nitrogen and hydrogen pathways[11,12]), as is typical for other cryospheric ecosystems[13,14]. Climate-induced glacier shrinkage is predicted to alter resource supply and stoichiometry in GFSs[15–17]. For instance, depending on underlying geology, decreasing subglacial weathering can reduce downstream P supply, whereas increasing contributions from non-glacial sources (for example, snowmelt and groundwater-fed streams) can increase downstream C and N concentrations[16,17]. However, how these shifts affect microbial energetics and related elemental fluxes in the world's GFSs currently remains unknown.

Limitations on microbial metabolism and related carbon use efficiency (CUE) are linked by the elemental stoichiometry of microbial biomass and resources[18,19]. This linkage is facilitated by the activity of extracellular enzymes that microorganisms produce to acquire C, N and P and which are regulated by kinetic and stoichiometric constraints[20]. Elemental stoichiometry constrains microorganisms to adapt their acquisition strategies to available resources, affecting their growth and respiration rates. The efficiency by which microorganisms allocate C to growth versus respiration is given by the CUE[19,21], making it a major intermediary to energy flow and the C cycle. Theoretical and empirical studies indicate that microbial CUE is responsive to environmental conditions. For instance, CUE may decrease with temperature if respiration responds more positively to temperature than growth, a relationship that appears inconsistent across terrestrial and aquatic ecosystems[22]. Furthermore, CUE can increase during algal blooms in pelagic systems when senescent algae exude labile organic matter to microbial heterotrophs[21]. Despite such algal–bacterial interactions in stream biofilms and the relevance of CUE as a microbial modulator of ecosystem-level C cycling, CUE remains poorly understood in stream ecosystems in general and in GFSs in particular.

Here we assessed microbial resource limitation and CUE across 154 GFSs sampled by the NOMIS Vanishing Glaciers project from some of Earth's major mountain ranges (Fig. 1a). Our analyses focused on the extracellular enzymatic activity (EEA) of microbial biofilms that inhabit benthic sediments. Benthic biofilms dominate microbial life and fulfil critical ecosystem processes[23]. Utilizing a space-for-time substitution approach[24], we explored how glacier shrinkage might affect resource supply and microbial energetics at a global scale by sampling GFSs under a wide range of glacier influence. We expected diminishing glacier influence to modulate changes in resource supply and microbial metabolism through shifting environmental conditions in GFSs. We used generalized additive mixed models (GAMMs) to disentangle effects from glacier influence and space (for example, mountain ranges), with spatial autocorrelation being inherent to datasets spanning spatial and environmental gradients. Space-for-time substitution was complemented by comparing within each GFS an upstream reach, as close to the glacier snout as possible, to a downstream reach, thereby capturing longitudinal chronosequences of deglaciation.

Resource supply in glacier-fed streams

Resource stoichiometry has a critical role in regulating ecosystem structure and function[25]. However, global-scale shifts in resource availability are difficult to predict owing to the limited spatial extent of currently available data. Our global dataset allowed us to identify effects of glacier influence on streamwater DOC, dissolved inorganic nitrogen (DIN) and soluble reactive phosphorus (SRP) concentrations. We used GAMMs to test combinations of parameters indicative of glacial influence (that is, glacier area, relative glacier cover, distance to the glacier) on the GFS ecosystem, selecting the best model through Bayes factor analysis (Methods). In all models, spatial effects accounted for a significant proportion of the variability in streamwater turbidity, temperature and SRP, reflecting regional differences (Fig. 1b and Extended Data Table 1).

In line with local and regional studies[7,26], our global survey underscores the pronounced oligotrophy of GFSs through consistently low DOC concentrations (median: 151 μg C l^{-1}; interquartile range (IQR): 103–239 μg C l^{-1}) (Extended Data Table 2). Low concentrations are due to the overall paucity of DOC sources in GFSs, combined with the effects of dilution from glacier run-off. Spatial structure explained most of the observed variation in DOC concentrations, and GAMMs did not retain glacial influence as a predictor (Extended Data Table 1).

Streamwater DIN concentrations (median: 95 μg N l^{-1}) varied across mountain ranges (IQR: 32–196 μg N l^{-1}) (Extended Data Table 2), with highest values in the Pamir and Tien Shan (median: 399 μg N l^{-1}; IQR: 238–521 μg N l^{-1}) and lowest values in Southwest Greenland (median: 16 μg N l^{-1}; IQR: 13–19 μg N l^{-1}). GAMMs failed to relate streamwater DIN concentration to glacier influence (Extended Data Table 1), in spite of controlling for regionality (Fig. 1b). Nitrogen, specifically nitrate, originates from various sources within the glacierized catchment, including atmospheric deposition[16,27] and geology[28], which vary regionally. Furthermore, once in the streamwater, microorganisms influence N concentrations and forms through uptake and transformation[16,27].

Streamwater SRP concentrations were relatively low across GFSs (median: 3 μg P l^{-1}; IQR = 1–7 μg P l^{-1}). Concentrations were highest in Ecuadorian Andes (median: 12 μg P l^{-1}; IQR = 8–29 μg P l^{-1}), Southwest Greenland (median: 9 μg P l^{-1}; IQR: 5–29 μg P l^{-1}), New Zealand Southern Alps (median: 7 μg P l^{-1}; IQR: 6–7 μg P l^{-1}) and Chilean Andes (median: 5 μg P l^{-1}; IQR: 3–12 μg P l^{-1}), whereas median SRP concentrations from the remaining regions were all below 2 μg P l^{-1}. These patterns are potentially attributable to the underlying geologies of GFSs. In fact, several of the mountain ranges with elevated median SRP concentrations feature historic volcanism (for example, Greenland's Disko Island, Ecuadorian and Chilean Andes) and are underlain by basalts. Indeed, streamwater SRP concentrations were positively correlated with sediment feldspar content (Spearman correlation, rho = 0.48, $P < 0.0001$). Thus, given the predominant geological origin of SRP in GFSs, it is not unexpected that the most parsimonious GAMM model retained only glacier area, which was positively related to SRP ($F = 0.719$, $P = 0.040$; Fig. 2c). Previous work has predicted declines in SRP concentration with glacier shrinkage[15,16], with the rationale that larger glaciers have an enhanced capacity to mechanically weather underlying bedrock and the subglacial hydrologic connectivity to flush these weathering products into GFSs. Our dataset, albeit with high regional variability, provides global-scale evidence for these previous predictions.

Patterns of streamwater DOC and nutrient concentrations translate into resource stoichiometries that vary widely across and within mountain ranges. Streamwater molar C:P varied from a median of 37.2 (IQR: 27.2–44.7) in New Zealand to 407 (IQR: 220–871) in the Pamir and Tien Shan. Streamwater molar C:N ranged from a median of 0.7 in the Russian Caucasus (IQR: 0.5–1.0) to 10.9 (IQR: 9.7–12.4) in Southwest Greenland. Lastly, median molar N:P ranged from 3.3 (IQR: 1.6–7.0) in Southwest Greenland to 546 (IQR: 138–855) in the Russian Caucasus. Together, overall median molar C:P, C:N and N:P ratios of our samples are 134 (IQR: 44–315), 1.8 (IQR: 0.8–5.4) and 72 (IQR: 12–274), respectively. Assuming that the canonical C:N:P Redfield ratio (that is, 106:16:1) indicates thresholds of nutrient limitation, our results suggest that N is not uniformly limiting in GFSs worldwide. On the contrary, streamwater resource ratios indicate widespread P limitation, and potentially also C limitation, in GFSs. Our global survey thus supports findings on P limitation in GFSs as reported from local studies[16,29]. Furthermore, given that SRP concentrations are expected to decline in the future as glaciers shrink, there is the potential to further exacerbate P limitation in GFSs globally.

Glacier-fed streams become greener

Benthic algae provide bioavailable organic matter to microbial heterotrophs in streams[30,31], which may be particularly important in GFSs largely devoid of terrestrial organic matter subsidies[15]. Besides nutrients, stream photoautotrophs are controlled by light availability[1], modulated by streamwater turbidity, and temperature[32]. Therefore,

https://doi.org/10.1038/s41561-024-01393-6

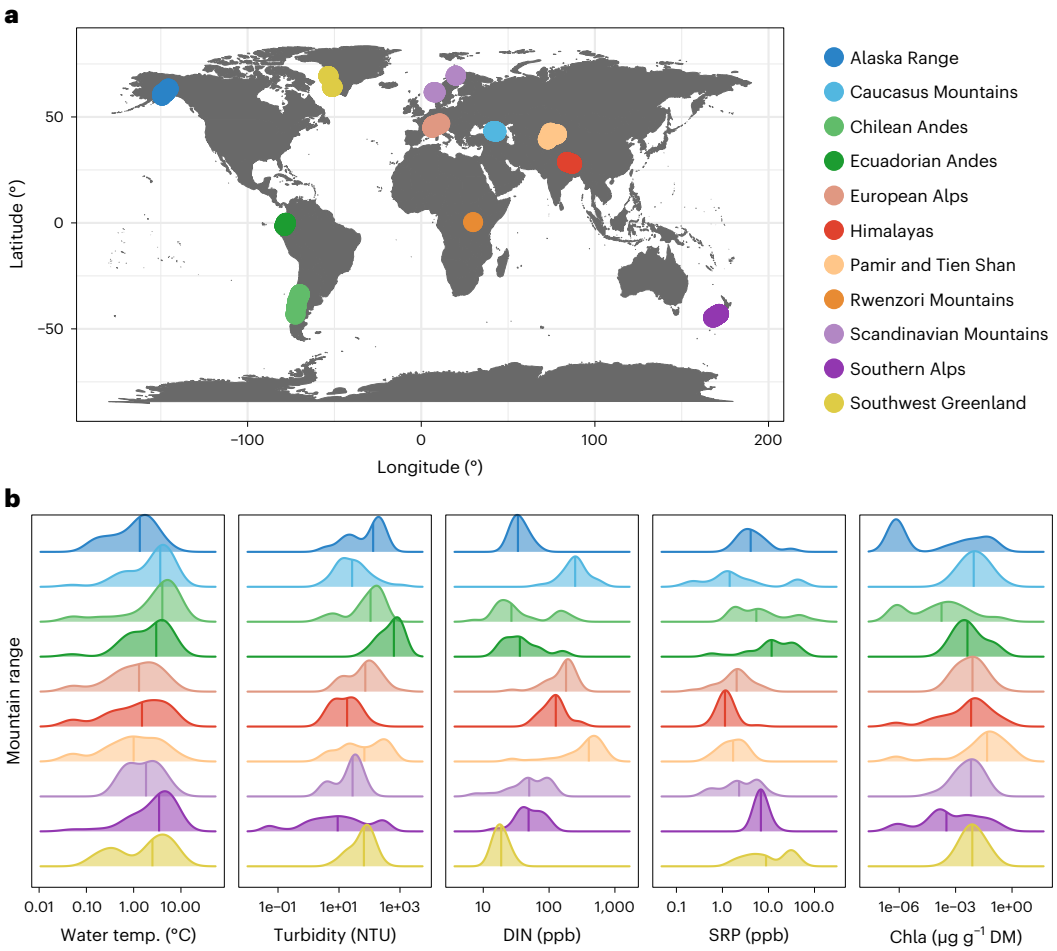

Fig. 1 | Geography and physico-chemical characteristics of the glacier-fed streams sampled by the Vanishing Glaciers project. a, Map showing the mountain ranges where glacier-fed streams (GFSs) were sampled. In each GFS, one upstream and one downstream reach was sampled for streamwater physico-chemical parameters; within each reach, three sediment patches were sampled for microbiological analyses. **b**, Density plots showing mountain-range-scale variability in important streamwater characteristics, including temperature, turbidity (nephelometric turbidity units; NTU), dissolved inorganic nitrogen (DIN), soluble reactive phosphorus (SRP) and chlorophyll-*a* (Chla) content of the dry mass (DM) of benthic sediments.

we used GAMMs to explore the glacier influence on these potential drivers across GFSs (Methods). Models revealed increasing streamwater turbidity and decreasing temperature with increasing glacier area (Fig. 2a,b); we also found that streamwater temperature increases with distance from glaciers (Extended Data Fig. 1 and Extended Data Table 1). The shrinkage of glaciers decreases their erosive forces, thereby reducing sediment production and streamwater turbidity[33,34]. Concurrently, glacier length recession allows for higher heat transfers into the streamwater from the atmosphere and streambed[35,36].

We found that benthic chlorophyll-*a*, a proxy for algal biomass, exhibited an inverse relationship with streamwater turbidity (Fig. 3 and Extended Data Table 1). Observable across a broad range of GFSs, this pattern is consistent with local-scale studies showing elevated primary production during periods of reduced turbidity and increased light availability[9,10]. The relationship also suggests that algal biomass will increase in GFSs beyond 'peak flow' (that is, when greater discharge is no longer generated by increasing glacier melt rates[37]), corresponding to a reduction in suspended sediments[34]. This space-for-time substitution approach across GFSs is corroborated by the significantly (Wilcoxon test, $P = 0.01$) higher benthic chlorophyll-*a* concentrations in downstream versus upstream reaches (median difference: 2.32×10^{-3} µg g^{-1} dry mass sediment; Extended Data Table 2). Altogether, patterns of benthic chlorophyll-*a* both across and within GFSs suggest impending 'greening' as glaciers shrink, analogous to the predicted 'greening' of high-mountain catchments[38]. Yet, the effect of 'greening' on GFS microbial energetics remains unknown.

Resource limitation and microbial metabolism

Given the apparent resource paucity in GFSs, we assessed potential resource limitations of the benthic microorganisms. We calculated threshold elemental ratios (TERs), which are the critical elemental C:P ($TER_{C:P}$) or C:N ($TER_{C:N}$) ratios at which the control of microbial metabolism switches from C to nutrient (N, P) limitation. TER was computed from the activities of the extracellular enzymes β-1,4-glucosidase (BG), leucine aminopeptidase (LAP), β-1,4-*N*-acetylglucosaminidase (NAG) and acid (alkaline) phosphatase (AP) (Methods).

Interestingly, GFS EEA profiles differ from those in soils, where the bulk of EEA-based stoichiometric research has been conducted[39]. In soils, LAP activity is typically low relative to BG, probably because of abundant polysaccharides derived from plant litter. However, in many streams, including GFSs, the opposite is true, with BG activity being consistently lower than LAP[18]. This pattern held in our global dataset, with the exception of the equatorial GFS of the Rwenzori Mountains, in which photoautotrophic processes dominated[40]. We attribute high relative LAP activity to its dual role in acquiring C and N from amino acids, for instance, provided by microorganisms and algae, which are more important organic matter sources in GFSs than plant litter. This dual nature is advantageous in a resource-limited ecosystem, given

https://doi.org/10.1038/s41561-024-01393-6

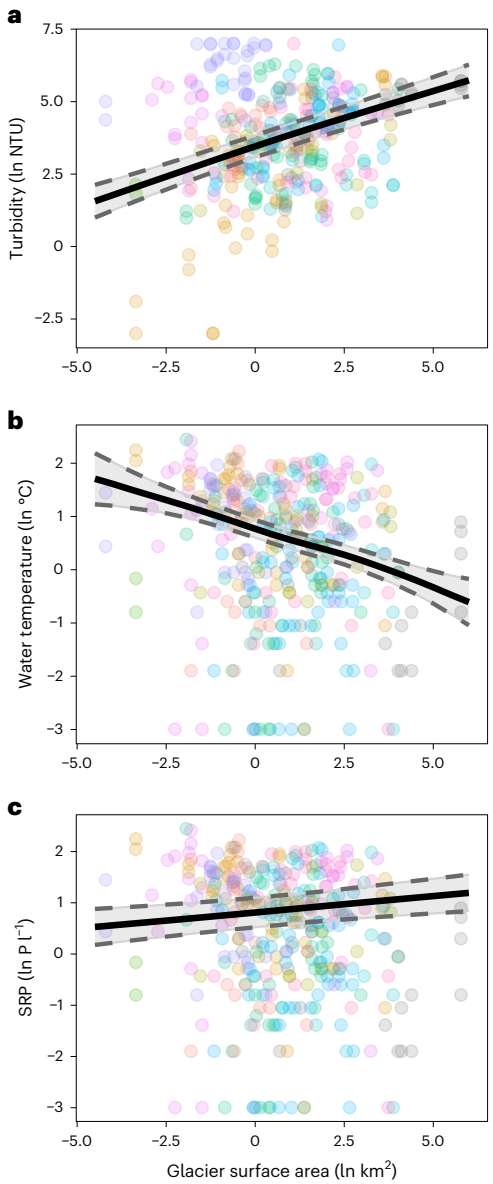

Fig. 2 | Shrinking glacier surface area leads to reductions in streamwater turbidity and soluble reactive phosphorus, increases in temperature. **a**,**b**, Generalized additive mixed models (GAMMs) accounting for the spatial structure of the data, and combined with a Bayes factor analysis to select relevant variables, revealed that streamwater turbidity increases with glacier area (n = 332) (**a**), whereas streamwater temperature decreases with glacier area (n = 338) (**b**). **c**, In terms of nutrients, soluble reactive phosphorus concentrations increase with glacier area (n = 301). Shown are the response curves with 95% prediction intervals. No adjustments for multiple comparisons were made, and reported P values are two sided; full GAMM results are provided in Extended Data Table 1. Colours represent the corresponding mountain ranges provided in the map in Fig. 1a.

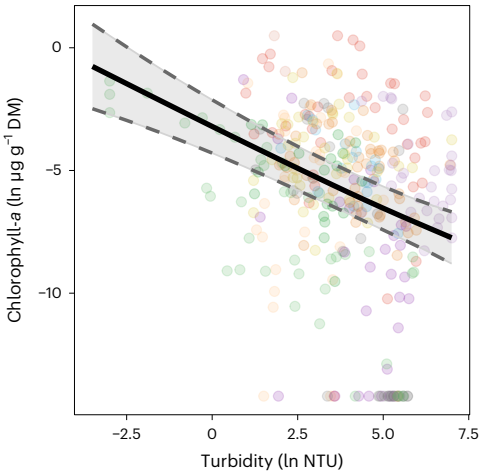

Fig. 3 | Streamwater turbidity affects the biomass of benthic primary producers in glacier-fed streams. GAMMs accounting for the spatial structure of the data, and combined with a Bayes factor analysis to select relevant variables, revealed that benthic chlorophyll-a is negatively related to streamwater turbidity (n = 302). Shown are the response curves with 95% prediction intervals. No adjustments for multiple comparisons were made, and reported P values are two sided; full GAMM results are provided in Extended Data Table 1. Colours represent the corresponding mountain ranges provided in the map in Fig. 1a.

the energetic costs to produce extracellular enzymes. However, it also makes it difficult to separate acquisition efforts for C and N individually, and we acknowledge this caveat for directly comparing $TER_{C:N}$ between GFSs and other systems, such as soils (Methods).

Across all GFSs, median $TER_{C:P}$ and $TER_{C:N}$ were 181 (IQR: 95.9–351.8) and 96.2 (IQR: 94.0–101.9), respectively (Fig. 4b,c and Extended Data Table 2). Overall, $TER_{C:P}$ varied more than $TER_{C:N}$ across mountain ranges. For instance, median $TER_{C:P}$ calculated for each region varied fourfold, from 71 in the Scandinavian Mountains to 286 in the Pamir and Tien Shan, whereas median $TER_{C:N}$ varied only 1.1 times from 93.9 in the Pamir and Tien Shan to 105.5 in Greenland (not taking into consideration the single Rwenzori GFS with a value of 479). These modelled $TER_{C:N}$ and $TER_{C:P}$ values were often higher than the Redfield ratio (C:N = 6.6, C:P = 106) and were approximately two and ten times larger, respectively, than those reported for river sediments[41]. Therefore, TER collectively indicates widespread C limitation, and to some extent also P limitation, of the benthic microbial metabolism, further supporting findings deduced from resource ratios.

We also investigated how biofilm TER may respond to environmental changes as glaciers shrink. Whereas GAMMs failed to explain $TER_{C:N}$, they retained chlorophyll-a to predict $TER_{C:P}$ (Fig. 5a and Extended Data Table 1). The negative relationship between $TER_{C:P}$ and chlorophyll-a across many different GFSs suggests that the 'greening' of GFSs relieves biofilms from C limitation and potentially pushes them towards P limitation. However, similar to cyanobacterial mats[42], GFS biofilms may recycle nutrients to mitigate effects of limitation.

Microbial carbon use efficiency

To further explore patterns and drivers of microbial energetics in GFSs, we derived CUE from stoichiometric modelling of the EEA[20], which produced a median value of 0.15 and varied across mountain ranges (IQR: 0.11–0.21; Fig. 4a and Extended Data Table 2). Because CUE can be estimated using various approaches, we first compared CUE derived from stoichiometric modelling to CUE derived from measured rates of bacterial C production and community respiration based on a subset of our samples (Methods). We found reasonable congruence between the independent approaches, with median values of 0.15 and 0.23 for CUE derived from stoichiometry and process rates, respectively (Extended Data Fig. 2). This comparison underscores the validity of stoichiometric modelling for estimating microbial CUE of GFS sediments.

Our estimates of CUE from global GFSs are comparable to median values from a wide range of aquatic ecosystems (median: 0.20; IQR: 0.04–0.61)[43], including temperate streams and rivers (0.016–0.299)[44], but are lower than the theoretical maximum bacterial CUE (0.6) and estimates for natural microbial communities in multi-resource-limited systems (0.3)[19]. Finally, they are also lower than the median CUE (0.36) reported from soil bacterial strains[45], typically biased towards microorganisms growing under optimal resource conditions. Therefore, globally low CUE in GFSs suggests a high degree of microbial maintenance metabolism and slow growth, probably due to limited resource supply in these ecosystems.

https://doi.org/10.1038/s41561-024-01393-6

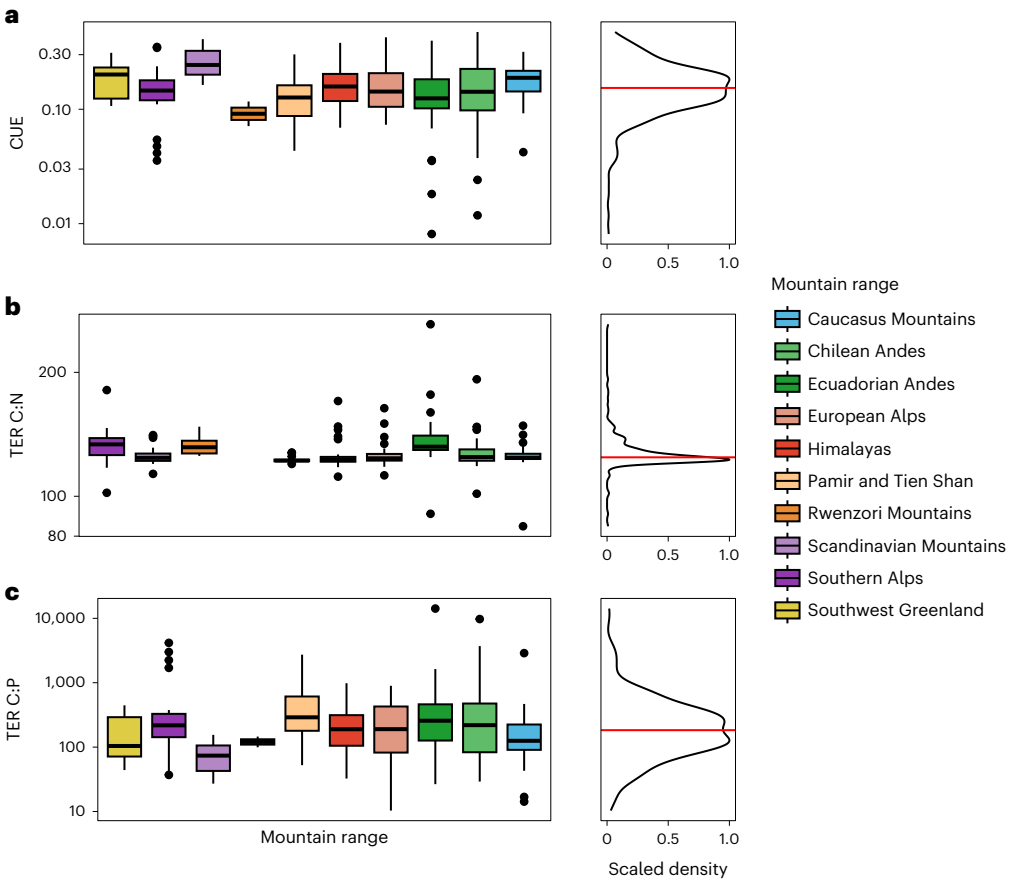

Fig. 4 | CUEs and TERs of glacier-fed streams across the world's major mountain ranges. a–**c**, Shown are boxplots for CUE ($n = 299$) (**a**), $TER_{C:N}$ ($n = 302$) (**b**) and $TER_{C:P}$ ($n = 303$) (**c**) for each of the ten mountain ranges. The lower and upper horizontal box boundaries indicate the interquartile range (IQR; denoting the 25th and 75th percentiles, respectively), and the middle horizontal lines represent the median. Vertical lines extend from each box to both the highest and lowest values (but no further than 1.5 times the IQR), and points outside this range are outliers. Shown to the right of each figure are scaled probability density functions representing the distributions for each of the three parameters, with red lines indicating the overall median values. Please note the difference in scale among the *y* axes.

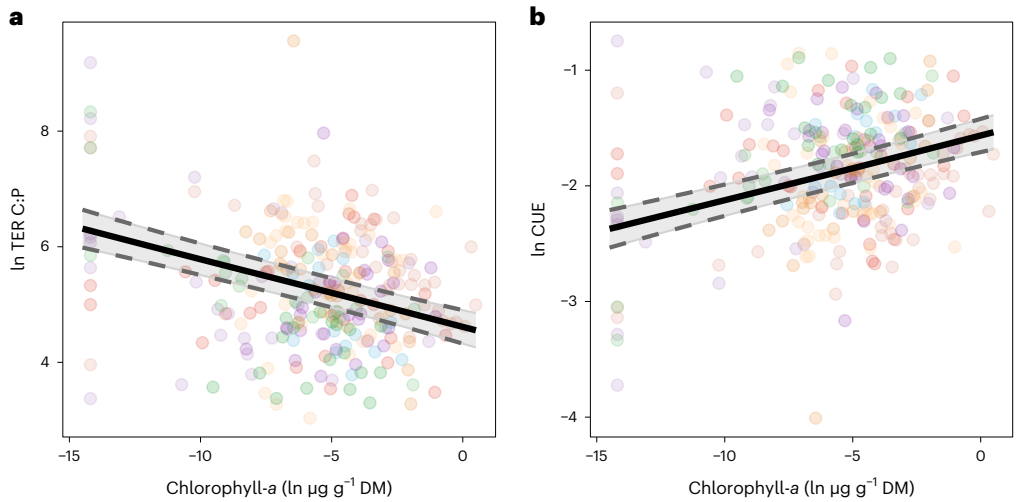

Fig. 5 | Nutrient limitation and CUE are related to benthic algal biomass. a,**b**, GAMMs accounting for the spatial structure of the data, combined with a Bayes factor analysis to select relevant variables, indicated that chlorophyll-*a* concentrations in the benthic sediments were negatively related to $TER_{C:P}$ ($n = 261$) (**a**) and positively related to CUE ($n = 261$) (**b**). Shown are the response curves with 95% prediction intervals. No adjustments for multiple comparisons were made, and reported *p* values are two sided; full GAMM results are provided in Extended Data Table 1. Colours represent the corresponding mountain ranges provided in the map (Fig. 1a).

To explore how CUE may change in global GFSs as glaciers shrink, we built GAMMs similar to those described above, but testing combinations of streamwater temperature, molar streamwater N:P and benthic chlorophyll-*a*, in addition to accounting for spatial structure (Methods and Extended Data Tables 1 and 3). The most parsimonious model retained chlorophyll-*a* as the only predictor for CUE (Fig. 5b). The significant and positive relationship between CUE and chlorophyll-*a* based on the 154 GFSs is consistent with the longitudinal differences in CUE within the GFSs. Specifically, we found significantly (Wilcoxon test, $P < 0.05$) higher CUE in downstream than upstream reaches (median difference in CUE: 0.03), reflecting the patterns of benthic chlorophyll-*a* reported for the same downstream gradients. These findings across and within GFSs suggest that augmented benthic autotrophic production may alleviate microbial heterotrophs from starvation, potentially through the provisioning of energy-rich exudates, thereby increasing their CUE[21]. That our models did not retain temperature as a predictor of CUE may be linked to the relatively low range of temperatures across GFSs globally (median: 1.95 °C; IQR: 0.6–4.0 °C) and the diel variation in temperature typical for many GFSs[9], to which communities are presumably adapted.

Next, we explored mechanisms that potentially underlie the observed patterns of microbial CUE in GFSs, specifically its components of growth (as bacterial C production) and respiration. As predicted by the growth rate hypothesis[25], more P is required as microbial growth rate increases to accommodate P-rich ribosomes and rRNA for rapid protein synthesis. Consistent with this hypothesis, we found that cell-specific phosphatase activity was positively correlated with CUE ($F = 22.2$, $P < 0.001$; Extended Data Fig. 3). This relationship further underscores the role of P limitation in driving microbial growth and related C fluxes in the world's GFSs. Another mechanism is the temperature dependence of growth and respiration. To test this effect, we constructed GAMMs with a spline accounting for algal biomass (chlorophyll-*a*) and tested a linear effect of relative temperature (Methods). We found a temperature dependence (Methods) of bacterial C production approximating 0.62 eV ($F = -4.654$, $P < 0.001$) (Extended Data Table 1), which is in agreement with temperature dependences reported for various C fluxes in aquatic ecosystems (for example, ref. 46) and stream ecosystem respiration (for example, refs. 47,48). Whereas this finding may appear unexpected given the narrow temperature range across GFSs, it suggests that microbial production will increase rapidly as streamwater temperatures rise and glaciers shrink. Yet, our model failed to establish a temperature dependence for respiration, which we tentatively attribute to the apparent dominance of maintenance metabolism. Additionally, we found no significant relationship indicating a temperature dependence of microbial CUE and cell-specific phosphatase (Extended Data Table 1).

In summary, our comprehensive study spanning the world's major mountain ranges unravels consistent trends of resource limitation in GFSs, despite regional and local differences, that corroborate predictions from conceptual models[16,17]. Our space-for-time substitutions, combined with elemental stoichiometry and microbial EEAs, indicate a 'green transition' with increasing primary production in GFSs that will relieve their microorganisms from energetic constraints as glacier influence diminishes. Increasing streamwater temperature will further accelerate microbial growth (as bacterial C production), which aligns with observations of enhanced degradation of organic matter in GFSs as glaciers shrink[49,50]. Shifting energy sources and microbial energetics are expected to have broader impacts for ecosystem functioning. In fact, faster growth would rely on a sufficiently high P supply, which may become increasingly limited as glaciers recede[16,17]. Metabolic interactions between bacteria and primary producers, as reported from GFS photoautotrophic biofilms[51], may counteract nutrient limitation through internal recycling. Our findings indicate that ecosystem C cycling will intensify in 'greener' GFSs, with yet unknown implications for regional C fluxes.

Online content

Any methods, additional references, Nature Portfolio reporting summaries, source data, extended data, supplementary information, acknowledgements, peer review information; details of author contributions and competing interests; and statements of data and code availability are available at https://doi.org/10.1038/s41561-024-01393-6.

References

1. Bernhardt, E. S. et al. Light and flow regimes regulate the metabolism of rivers. *Proc. Natl Acad. Sci. USA* **119**, e2121976119 (2022).
2. Battin, T. J. et al. River ecosystem metabolism and carbon biogeochemistry in a changing world. *Nature* **613**, 449–459 (2023).
3. Vannote, R. L., Wayne Minshall, G., Cummins, K. W., Sedell, J. R. & Cushing, C. E. The river continuum concept. *Can. J. Fish. Aquat. Sci.* **37**, 130–137 (1980).
4. Webster, J. R. & Meyer, J. L. Organic matter budgets for streams: a synthesis. *J. North Am. Benthol. Soc.* **16**, 141–161 (1997).
5. Rosemond, A. D. et al. Experimental nutrient additions accelerate terrestrial carbon loss from stream ecosystems. *Science* **347**, 1142–1145 (2015).
6. Catalán, N. et al. Behind the scenes: mechanisms regulating climatic patterns of dissolved organic carbon uptake in headwater streams. *Glob. Biogeochem. Cycles* **32**, 1528–1541 (2018).
7. Singer, G. A. et al. Biogeochemically diverse organic matter in Alpine glaciers and its downstream fate. *Nat. Geosci.* **5**, 710–714 (2012).
8. Hood, E., Battin, T. J., Fellman, J., O'neel, S. & Spencer, R. G. M. Storage and release of organic carbon from glaciers and ice sheets. *Nat. Geosci.* **8**, 91–96 (2015).
9. Uehlinger, U., Robinson, C. T., Hieber, M. & Zah, R. The physico-chemical habitat template for periphyton in alpine glacial streams under a changing climate. *Hydrobiologia* **657**, 107–121 (2010).
10. Boix Canadell, M. et al. Regimes of primary production and their drivers in Alpine streams. *Freshwater Biol.* **66**, 1449–1463 (2021).
11. Ren, Z., Gao, H., Elser, J. J. & Zhao, Q. Microbial functional genes elucidate environmental drivers of biofilm metabolism in glacier-fed streams. *Sci. Rep.* **7**, 12668 (2017).
12. Michoud, G. et al. Unexpected functional diversity of stream biofilms within and across proglacial floodplains despite close spatial proximity. *Limnol. Oceanogr.* https://doi.org/10.1002/lno.12415 (2023).
13. Bourquin, M. et al. The microbiome of cryospheric ecosystems. *Nat. Commun.* **13**, 3087 (2022).
14. Margesin, R. & Collins, T. Microbial ecology of the cryosphere (glacial and permafrost habitats): current knowledge. *Appl. Microbiol. Biotechnol.* **103**, 2537–2549 (2019).
15. Milner, A. M. et al. Glacier shrinkage driving global changes in downstream systems. *Proc. Natl Acad. Sci. USA* **114**, 9770–9778 (2017).
16. Ren, Z., Martyniuk, N., Oleksy, I. A., Swain, A. & Hotaling, S. Ecological stoichiometry of the mountain cryosphere. *Front. Ecol. Evol.* **7**, 760 (2019).
17. Elser, J. J. et al. Key rules of life and the fading cryosphere: impacts in alpine lakes and streams. *Glob. Change Biol.* **26**, 6644–6656 (2020).
18. Sinsabaugh, R. L. & Shah, J. J. F. Ecoenzymatic stoichiometry and ecological theory. *Annu. Rev. Ecol. Evol. Syst.* **43**, 313–343 (2012).
19. Sinsabaugh, R. L., Manzoni, S., Moorhead, D. L. & Richter, A. Carbon use efficiency of microbial communities: stoichiometry, methodology and modelling. *Ecol. Lett.* **16**, 930–939 (2013).

20. Sinsabaugh, R. L., Hill, B. H. & Follstad Shah, J. J. Ecoenzymatic stoichiometry of microbial organic nutrient acquisition in soil and sediment. *Nature* **462**, 795–798 (2009).
21. del Giorgio, P. A. & Cole, J. J. Bacterial growth efficiency in natural aquatic systems. *Annu. Rev.* **29**, 503–541 (1998).
22. Allison, S. D., Wallenstein, M. D. & Bradford, M. A. Soil-carbon response to warming dependent on microbial physiology. *Nat. Geosci.* **3**, 336–340 (2010).
23. Battin, T. J. et al. The ecology and biogeochemistry of stream biofilms. *Nat. Rev. Microbiol.* **14**, 251–263 (2016).
24. Pickett, S. T. A. in *Long-Term Studies in Ecology* (ed. Likens, G.E.) 110–135 (Springer, 1989).
25. Sterner, R. W., Elser, J. J. *Ecological Stoichiometry: The Biology of Elements from Molecules to the Biosphere* (Princeton Univ. Press, 2002).
26. Hood, E. & Scott, D. Riverine organic matter and nutrients in southeast Alaska affected by glacial coverage. *Nat. Geosci.* **1**, 583–587 (2008).
27. Slemmons, K. E. H., Saros, J. E. & Simon, K. The influence of glacial meltwater on alpine aquatic ecosystems: a review. *Environ. Sci. Process. Impacts* **15**, 1794–1806 (2013).
28. Houlton, B. Z., Morford, S. L. & Dahlgren, R. A. Convergent evidence for widespread rock nitrogen sources in Earth's surface environment. *Science* **360**, 58–62 (2018).
29. Ren, Z., Gao, H., Luo, W. & Elser, J. J. C:N:P stoichiometry in six distinct habitats of a glacier terminus in the source area of the Yangtze River. *Biogeochemistry* **158**, 181–194 (2022).
30. Kaplan, L. A. & Bott, T. L. Diel fluctuations in bacterial activity on streambed substrata during vernal algal blooms: effects of temperature, water chemistry, and habitat. *Limnol. Oceanogr.* **34**, 718–733 (1989).
31. Wagner, K., Bengtsson, M. M., Findlay, R. H., Battin, T. J. & Ulseth, A. J. High light intensity mediates a shift from allochthonous to autochthonous carbon use in phototrophic stream biofilms. *J. Geophys. Res. Biogeosci.* **122**, 1806–1820 (2017).
32. Song, C. et al. Continental-scale decrease in net primary productivity in streams due to climate warming. *Nat. Geosci.* **11**, 415–420 (2018).
33. Anderson, S. P. Biogeochemistry of glacial landscape systems. *Annu. Rev. Earth Planet. Sci.* **35**, 375–399 (2007).
34. Zhang, T. et al. Warming-driven erosion and sediment transport in cold regions. *Nat. Rev. Earth Environ.* **3**, 832–851 (2022).
35. Cadbury, S. L., Hannah, D. M., Milner, A. M., Pearson, C. P. & Brown, L. E. Stream temperature dynamics within a New Zealand glacierized river basin. *River Res. Appl.* **24**, 68–89 (2008).
36. Khamis, K., Brown, L. E., Milner, A. M. & Hannah, D. M. Heat exchange processes and thermal dynamics of a glacier-fed alpine stream. *Hydrol. Processes* **29**, 3306–3317 (2015).
37. Huss, M. & Hock, R. Global-scale hydrological response to future glacier mass loss. *Nat. Clim. Change* **8**, 135–140 (2018).
38. Rumpf, S. B. et al. From white to green: snow cover loss and increased vegetation productivity in the European Alps. *Science* **376**, 1119–1122 (2022).
39. Sinsabaugh, R. L. et al. Stoichiometry of soil enzyme activity at global scale. *Ecol. Lett.* **11**, 1252–1264 (2008).
40. Michoud, G. et al. The dark side of the moon: first insights into the microbiome structure and function of one of the last glacier-fed streams in Africa. *R. Soc. Open Sci.* **10**, 230329 (2023).
41. Sinsabaugh, R. L., Follstad Shah, J. J., Hill, B. H. & Elonen, C. M. Ecoenzymatic stoichiometry of stream sediments with comparison to terrestrial soils. *Biogeochemistry* **111**, 455–467 (2012).
42. Jentzsch, L., Grossart, H.-P., Plewe, S., Schulze-Makuch, D. & Goldhammer, T. Response of cyanobacterial mats to ambient phosphate fluctuations: phosphorus cycling, polyphosphate accumulation and stoichiometric flexibility. *ISME Commun.* **3**, 6 (2023).
43. Manzoni, S. et al. Optimal metabolic regulation along resource stoichiometry gradients. *Ecol. Lett.* **20**, 1182–1191 (2017).
44. Hill, B. H., Elonen, C. M., Herlihy, A. T., Jicha, T. M. & Mitchell, R. M. A synoptic survey of microbial respiration, organic matter decomposition, and carbon efflux in U.S. streams and rivers. *Limnol. Oceanogr.* **62**, S147–S159 (2017).
45. Smith, T. P., Clegg, T., Bell, T. & Pawar, S. Systematic variation in the temperature dependence of bacterial carbon use efficiency. *Ecol. Lett.* **24**, 2123–2133 (2021).
46. Yvon-Durocher, G., Jones, J. I., Trimmer, M., Woodward, G. & Montoya, J. M. Warming alters the metabolic balance of ecosystems. *Philos. Trans. R. Soc. B Biol. Sci.* **365**, 2117–2126 (2010).
47. Perkins, D. M. Temperature effects on community size structure: the value of large-scale biomonitoring programs. *Glob. Change Biol.* **28**, 687–689 (2022).
48. Acuña, V., Wolf, A., Uehlinger, U. & Tockner, K. Temperature dependence of stream benthic respiration in an Alpine river network under global warming. *Freshwater Biol.* **53**, 2076–2088 (2008).
49. Fell, S. C. et al. Fungal decomposition of river organic matter accelerated by decreasing glacier cover. *Nat. Clim. Change* **11**, 349–353 (2021).
50. Kohler, T. J. et al. Glacier shrinkage will accelerate downstream decomposition of organic matter and alters microbiome structure and function. *Glob. Change Biol.* **28**, 3846–3859 (2022).
51. Busi, S. B. et al. Genomic and metabolic adaptations of biofilms to ecological windows of opportunity in glacier-fed streams. *Nat. Commun.* **13**, 2168 (2022).

Vanishing Glaciers Field Team

Michael Styllas[1], Martina Schön[1], Matteo Tolosano[1], Vincent de Staercke[1], Tyler J. Kohler[1,2], Hannes Peter[1] & Tom J. Battin[1]

Methods

Sampling and streamwater chemical analyses

From 2019 to 2022, we sampled 169 GFSs from 11 major mountain ranges, including the Southern Alps of New Zealand (20 GFSs), the Nuuk and Disko Island (Qeqertarsuaq) areas of west and southwest Greenland (10 GFSs), the Ecuadorian (15 GFSs) and Chilean (15 GFSs) Andes, the Caucasus Mountains of Russia (19 GFSs), the Lyngen Alps and Jotunheim Mountains of Norway (referred to as Scandinavian Mountains; 10 GFSs), the European Alps (27 GFSs), the Himalayas (17 GFSs), the Tien Shan and Pamir of Kyrgyzstan (20 GFSs), the Alaska Range of North America (15 GFSs) and the Rwenzori Mountains in Uganda (1 GFS). The GFSs cover a wide range of latitudes, elevations, glacier sizes and geologies[52].

Samples were predominantly collected during vernal and autumnal 'windows of opportunity' (that is, temporal periods flanking peak summer icemelt and winter freeze-up and snow cover, collectively associated with greater biofilm biomass[9,10]), and we abstained from sampling heavily debris-covered glaciers and rock glaciers and GFSs with proglacial lakes, debris flows or non-glacial tributaries upstream of the sampling site. For each GFS, we sampled one upstream reach as close to the glacier snout as possible (median distance from snout: 76 m; IQR: 29–301 m) and one downstream reach (median distance from snout: 706 m from glacier; IQR: 336–1,280 m) to encompass a longitudinal gradient of the GFS environment. The median distance between upstream and downstream reaches was 515 m (IQR: 236–933 m) and ranged from 22 to 3,936 m. The Alaskan GFSs were included for nutrient resource analyses but not for microbial energetics.

Streamwater turbidity was measured with a portable turbidity meter (Turb 430 IR, WTW). Streamwater samples were further collected for the measurement of nutrient concentrations in both upstream and downstream reaches, with the exception of New Zealand, where only the upstream reaches were sampled. Nutrient samples were collected by filtering water through ashed GF/F filters (Whatman) into acid-washed Nalgene HDPE bottles and were frozen within 24 h. Nutrient concentrations were measured on a Lachat QuikChem 8500 flow injection analyser and included nitrite (NO^{2-}; QuikChem Method 10-107-05-1-C, detection limit: 1.6 µg N l^{-1} as NO_2^-), nitrite/nitrate ($NO_2^- + NO_3^-$; 10-107-04-1-B, detection limit: 0.3 µg N l^{-1}), ammonium (NH_4^+; 10-107-06-3-D, detection limit: 1 µg N l^{-1} as NH_3) and soluble reactive phosphorus (SRP; 10-115-01-1-M, detection limit: 0.1 µg P l^{-1} as PO_4^{3-}). Dissolved inorganic nitrogen (DIN) was calculated by adding together N-NH_4^+, N-NO_2^- and NO_3^-, which was then used in streamwater C:N and N:P ratios. For all nutrient species, values reflect concentrations of N and P (rather than NO_x and PO_4^{3-} molecules), and values were corrected by the molar mass of each element before calculating molar C:N:P ratios. Samples for DOC were collected at upstream reaches only and filtered through ashed GF/F (Whatman) filters, stored at 4 °C in acid-washed and combusted amber glass vials and measured on a Sievers M5310 C TOC Analyser (Veolia); accuracy of the DOC measurements was ±2%, precision <1% RSD and detection limit 2 µg C l^{-1}. As DOC samples were collected from upstream reaches only, streamwater C:N and C:P ratios refer to upstream reaches.

In each GFS reach, we sampled sediment-associated biofilms from three sediment patches within a perimeter of 5 to 10 m. Benthic sediments (the upper 5-cm layer of the streambed) were removed and sorted using graded sieves (250 µm to 3.15 mm size fraction) to retain the sandy fraction. Sandy sediments contribute the most surface area to the overall streambed, and their ubiquity facilitates comparison within and among GFSs. All sampling equipment was flame-sterilized in the field. Aliquots for the analysis of chlorophyll-*a* and extracellular enzyme activities were transferred into cryovials and flash frozen in the field using liquid nitrogen. Other aliquots were retained for the in situ determination of bacterial C production and community respiration. A subset of the sampled sediment was further retained to characterize mineralogy and was analysed using an X-TRA ThermoARL Diffractometer. Errors varied between 5% and 10% for the phyllosilicates and 5% for grain minerals. Raw data files were generated and transformed into calculated files by WinXRD 2.0-6 (Thermo Fisher). Relative abundances of the main mineral groups were estimated from the raw counts of mica, chlorite, amphibole, feldspars, calcite and quartz divided by the sum of counts.

Benthic chlorophyll-*a*

We extracted chlorophyll-*a* from the benthic sediments by adding 90% ethanol, extracting in a hot water bath (78 °C) for 10 min and incubating in the dark at 4 °C for 24 h. Following incubation, samples were vortexed, centrifuged (max. speed for 5 min) and read in a high-sensitivity plate reader (BioTek Synergy H1) at 436/680 ex/em wavelengths. Chlorophyll-*a* concentrations were normalized by the dry mass of sediment (µg Chla g^{-1} dry mass).

Bacterial abundance

Bacterial abundance was determined as done previously[53]. In brief, 2.5–3 g of wet sediment were fixed in situ in filter-sterilized paraformaldehyde/glutaraldehyde solution for each patch and flash frozen on dry ice pending analysis. Microbial cells were detached through shaking and sonication (Sonifier 450, Branson, 1 min, 60% duty cycle, output 5) in paraformaldehyde/glutaraldehyde solution supplemented with sodium pyrophosphate (final concentration of 0.025 mM). Extracts were transferred into a sterile Eppendorf tube and centrifuged to pellet larger sediment and debris particles. The supernatant was then diluted tenfold in paraformaldehyde/glutaraldehyde solution and stained with SYBR Green before being analysed on a NovoCyte flow cytometer (ACEA Biosciences) equipped with a 488 nm laser. Results were corrected for various dilution factors and for normalized to sediment dry mass (cells g^{-1} dry mass).

Extracellular enzymatic activities

Extracellular enzyme activity (EEA) was quantified by measuring potential activities of α-1,4-glucosidase (AG), β-1,4-glucosidase (BG, leucine aminopeptidase (LAP), β-1,4-*N*-acetylglucosaminidase (NAG) and acid (alkaline) phosphatase (AP) using fluorescent 4-methylumbelliferone (MUF) and 7-amino-4-methylcoumarin (AMC)-linked substrates (4-MUF-α-D-glucoside, 4-MUF-β-D-glucoside, L-leucine-7-amino-4-AMC, 4-MUF-*N*-acetyl-β-D-glucosaminide and 4-MUF-phosphate, respectively). All substrates were dissolved in artificial streamwater (pH adjusted to 7.5) at a concentration of 0.3 µM, based on previous work[53]. Approximately 1 g (wet weight) of sediment was transferred to pre-weighed centrifuge tubes, and 4 ml of MUF and AMC-linked substrates (at 4 °C) were added to the samples and allowed to incubate for 1.5 to 2 h in the dark on a shaker at 4 °C. In addition to assays, we incubated reference standards of MUF and AMC with several controls for each sediment sample: a blank (artificial streamwater only), a matrix control (sediment plus artificial streamwater), a quench control (sediment plus MUF or AMC reference standard) and a deactivated control (sediment boiled for 30 min before adding substrate). Following incubations, 2 ml of glycine buffer (pH10.4) was quickly added to all tubes (2:1 sample:buffer vol:vol ratio) to raise the pH and halt product generation. Samples were vortexed, centrifuged and the supernatant transferred to black 96-well plates (Corning, flat bottom, polystyrene non-binding surface) before fluorescences were read on a BioTek Synergy H1 high-sensitivity plate reader at 365/455 excitation/emission wavelengths for MUF and 364/445 excitation/emission wavelengths for AMC. Following analyses, sediments were dried and weighed, and enzymatic activities (nmol h^{-1} g^{-1} dry mass) were calculated using equations in ref. 53.

Bacterial carbon production

Bacterial C production (BCP) was determined according to ref. 54. In brief, we incubated sediment samples (2.5 to 3 g) for 2 h in the field with

30 nM [^{3}H]leucine (specific activity: 149.0 Ci mmol^{-1}, PerkinElmer) in the dark at in situ stream temperature. The incorporation was halted with the addition of formaldehyde (3.7% final concentration). Killed controls were run in parallel to quantify background signals. In the laboratory, microbial cells were detached from the sediments using vortexing and mild sonication (Sonorex Super RK512, 35 kHz, 225/450 W, Bandelin). Proteins were extracted from cells by adding 1.53 ml of trichloroacetic acid (15% TCA), followed by incubation in a water bath (95 °C, 30 min) and cooling on ice (30 min) to coagulate proteins. Samples were then filtered (100 mbar, Vacuubrand) through 0.2 µm polycarbonate filters (Isopore, GTTP02500, Millipore, Merck) and rinsed twice with ice-cold 5% TCA. Finally, samples were transferred into 14 ml of scintillation cocktail (PerkinElmer, Optiphase Hisafe 3), and disintegrations per minute were measured for 5 min in a low-activity liquid scintillation counter (Tri-Carb 4910 TR, Perkin Elmer) after a 30-sec delay. Data were converted to leucine incorporation using its specific activity, and bacterial protein production was calculated according to refs. 55,56. From this, BCP was calculated by multiplying by the protein-to-cell C ratio (0.86). Some raw data showed evidence of quenching (that is, signal attenuation), and an external standard incorporated into the scintillation counter (133 Ba) was used to make corrections using the external standard ratio method[55]. Blanks for each sample were inspected separately, and if an outlier was observed, it was replaced by the mean of the other blanks in the dataset. Calculated rates were subsequently normalized by the dry mass of the sediment (ng C h^{-1} g^{-1} dry mass).

Microbial respiration

The respiration of the microbial community attached to the sediments was determined in situ using multi-channel optical FireSting$^{(R)}$-Pro (PyroScience Germany) systems integrated into custom-made respiration chambers. These chambers consisted of borosilicate tubes with planar optodes connected to fibre-optic sensors. Each tube (two per sediment patch) received sandy sediments (up to 10 g) and was further filled with sterile-filtered (0.2 µm, Millipore) GFS water with no air bubble inclusions. As for BCP, the respiration chamber was incubated in the dark and fully submerged in the GFS to ensure in situ temperatures. After an equilibration period, we monitored oxygen concentration and temperature every 15 sec for at least 2 h. Temperature-corrected oxygen concentrations were extracted, and outliers were removed from the time series using an R script. More specifically, variation in temperature (>2 °C) during the incubation affected the internal temperature compensation and consequently measurements were discarded. Inspection of replicated measurements revealed deviations that we attribute to small air bubbles in the vials. Such measurements were also discarded. Moreover, the harsh field conditions eventually led to malfunctioning of the system. Nevertheless, at least one respiration datum from 88% of the GFSs (136/154) and 81% of the reaches (251/308) were retained for further analysis. Respiration rates were calculated from the slope of the oxygen concentration over time and normalized by the dry weight of the sediment (mg O_2 h^{-1} g^{-1} dry mass) and averaged per reach.

Threshold elemental ratios and carbon use efficiency

By comparing different enzyme classes used to acquire different elements, stoichiometric models can be formulated to calculate threshold elemental ratios (TER), which provide an indication of the ratio at which these heterotrophic metabolic processes are limited by nutrients and/or energy[20,25]. Because of the high-protein peaks observed in the DOM of alpine streams[7], and coupled with the high LAP activities previously reported for GFS sediments[53], we postulate that LAP is probably generated to capitalize on microbially derived organic compounds and to efficiently acquire both N and C. Thus, we have reorganized the equations formulated by ref. 20 to also include LAP as a C-acquiring EEA in models alongside BG, as recommended by refs. 18,57. Threshold elemental ratios ($TER_{C:X}$) were first calculated based on equations formulated by ref. 20 and as reproduced by ref. 58:

$$TER_{C:N} = \frac{\left(\frac{BG + LAP}{LAP + NAG}\right)/B_{C:N}}{n_0} \quad (1)$$

$$TER_{C:P} = \frac{\left(\frac{BG + LAP}{AP}\right)/B_{C:P}}{p_0} \quad (2)$$

where $B_{C:X}$ is the C to nutrient ratio of microbial cells, which were taken from ref. 59 (C:N = 8.6 and C:P = 60) and n_0 and p_0 are scalars determined by finding the intercept between C-acquiring EEA (BG and LAP) and N-acquiring (NAG and LAP) and P-acquiring (AP) EEA[58]. Scalars were calculated using the entire dataset so as not to induce differences as a function of mountain range and so on. Once TER values were calculated, they were used to calculate CUE by using the equation given in refs. 19,60:

$$CUE = \left(\left(\frac{(B_{C:N} \times A_N)}{TER_{C:N}}\right) \times \left(\frac{(B_{C:P} \times A_P)}{TER_{C:P}}\right)\right)^{0.5} \quad (3)$$

where A_X is the assimilation efficiency of N or P (0.9). Finally, microbial CUE was also calculated as the ratio of BCP to the sum of BCP and respiration (R):

$$CUE = \frac{BCP}{(BCP + R)} \quad (4)$$

Statistical analyses

All statistics were performed using R (version 4.1.1)[61]. When necessary to achieve normality, data were log-transformed (natural logarithm) after addition of a value equal to 0.5 times the lowest datum for a given variable. For CUE, $TER_{C:N}$ and $TER_{C:P}$, outliers were discarded if their values were more than three standard deviations away from the mean.

The statistical framework of this study was implemented as follows: we constructed spatial splines to account for spatial autocorrelation at the regional scale (that is, mountain ranges) and included random effects to correct for correlations between upstream and downstream reaches that were sampled within each GFS. Specifically, we used generalized additive mixed models (GAMM function; mgcv R package) with a spatial spline (using latitude and longitude with parameters set as bs = 'sos', $m = 1$ and $k = -1$) to account for spatial autocorrelation at the regional scale. To remove autocorrelation arising within a GFS (between upstream and downstream reaches), a random effect with the 'corCAR1(form = ~ 1 | GFS)' correlation structure was used. To compare different combinations of predictor variables, and to identify the best-fitting model, a tensor (parameters set as bs = 'ts' and $k = 5$) was used, combined with a Bayes factor analysis using the 'test_bf()' command from the performance package[62]. Models encompassing all possible combinations of predictors in the tensors were compared against a null model based solely on the spatial spline. The best model, when compared to the null, was retained. If no model had a Bayes factor ≥3, the null model was retained.

To calculate the temperature dependence of bacterial carbon production, respiration, CUE and cell-specific AP, another set of GAMM models was created. These models included the inverse relative water temperature as a dependent variable and accounted for chlorophyll-a as a smoothed term. Spatial splines and random effects, as described previously, were not used in these models. Dependent variables were natural log-transformed, and the linear slope estimate between the dependent variables and the inverse relative water temperature was used to estimate temperature dependence. Inverse relative water temperature was calculated according to ref. 49:

$$\text{inverse relative water temperature} = \left(\frac{1}{K_B \times \text{Temp}}\right) - \left(\frac{1}{K_B \times \text{Temp}_0}\right) \quad (5)$$

where K_B is the Boltzmann constant (0.0000862), Temp is the measured water temperature (K) and Temp_0 is 283.15 (that is, temperatures normalized to 10 °C).

A brief summary of the model structure for a given class of dependent variable is provided in Extended Data Table 3 and below:

1. Physical template models: the optimal combination of glaciological parameters (distance from the glacier, percent glacier coverage and glacier area, all represented in a tensor) was selected based on a Bayes factor analysis to elucidate the parameters affecting streamwater turbidity, water temperature, DOC, SRP and DIN.
2. Chlorophyll-*a* model: the most suitable combination of streamwater characteristics (turbidity, temperature, SRP and DIN, all represented in a tensor) was identified via a Bayes factor analysis to explain variations of chlorophyll-*a* concentrations.
3. CUE and TER models: the optimal combination of streamwater temperature, dissolved N:P ratios and benthic chlorophyll-*a* (all included a tensor) was determined based on a Bayes factor analysis to explain CUE, $\text{TER}_{C:N}$ and $\text{TER}_{C:P}$.
4. Cell-specific AP versus CUE: cell-specific AP, represented as a tensor, served as a predictor for CUE.
5. Temperature dependence models: inverse relative water temperature, along with chlorophyll-*a* (represented as a spline), were used to explain log-transformed values for respiration, bacterial carbon production, CUE and cell-specific AP.

Data availability

All data have been deposited in *Zenodo* at https://doi.org/10.5281/zenodo.10469376.

Code availability

All the data and code needed to reproduce this study can be found on the following Github repository: https://github.com/Mass23/EmergentResponses, with information on how to run analyses and the dependencies needed.

References

52. Battin, T. J. et al. Towards a global biogeography of the glacier-fed stream benthic microbiome. Preprint at *Research Square* https://doi.org/10.21203/rs.3.rs-2697617/v1 (2023).
53. Kohler, T. J. et al. Patterns and drivers of extracellular enzyme activity in New Zealand glacier-fed streams. *Front. Microbiol.* **11**, 591465 (2020).
54. Fischer, H. & Pusch, M. Use of the [14 C]leucine incorporation technique to measure bacterial production in river sediments and the epiphyton. *Appl. Environ. Microbiol.* **65**, 4411–4418 (1999).
55. Simon, M. & Azam, F. Protein content and protein synthesis rates of planktonic marine bacteria. *Mar. Ecol. Prog. Ser.* **51**, 201–213 (1989).
56. Marxsen, J. Measurement of bacterial production in stream-bed sediments via leucine incorporation. *FEMS Microbiol. Ecol.* **21**, 313–325 (1996).
57. Mori, T. Does ecoenzymatic stoichiometry really determine microbial nutrient limitations? *Soil Biol. Biochem.* **146**, 107816 (2020).
58. Tapia-Torres, Y., Elser, J. J., Souza, V. & García-Oliva, F. Ecoenzymatic stoichiometry at the extremes: how microbes cope in an ultra-oligotrophic desert soil. *Soil Biol. Biochem.* **87**, 34–42 (2015).
59. Cleveland, C. C. & Liptzin, D. C:N:P stoichiometry in soil: is there a 'Redfield ratio' for the microbial biomass? *Biogeochemistry* **85**, 235–252 (2007).
60. Sinsabaugh, R. L. et al. Stoichiometry of microbial carbon use efficiency in soils. *Ecol. Monogr.* **86**, 172–189 (2016).
61. R Core Team. *R: A Language and Environment for Statistical Computing* (R Foundation for Statistical Computing, 2021).
62. Lüdecke, D., Ben-Shachar, M., Patil, I., Waggoner, P. & Makowski, D. performance: An R package for assessment, comparison and testing of statistical models. *J. Open Source Softw.* **6**, 3139 (2021).

Acknowledgements

This research was supported by The NOMIS Foundation project 'Vanishing Glaciers' awarded to T.J.B. T.J.K. received additional support from the Charles University project PRIMUS/22/SCI/001 and the Charles University Research Centre programme number 204069. We are most grateful to A. McIntosh and L. Morris in New Zealand; J. Abermann and T. Juul-Pedersen in Greenland; O. Solomina and T. Kuderina Maratovna in Russia; V. Crespo-Pérez and P. Andino Guarderas in Ecuador; J. Yde and S. Leth Jørgensen in Norway; S. Sharma and P. Joshi in Nepal; N. Shaidyldaeva-Myktybekovna and R. Kenzhebaev in Kyrgyzstan; J. Nattabi Kigongo, R. Nalwanga and C. Masembe in Uganda; M. Gonzaléz and J. Luis Rodriguez in Chile and C. Kuhle and P. Tomco in Alaska for their logistical support. This work would not have been possible without the tireless efforts of the many porters and guides in Nepal, Uganda and Kyrgyzstan. T. Adatte helped with mineral analysis. We thank L. Ezzat, S. Busi, G. Michoud and A. Robison for discussions and T. Dupont, A. Bonetti, R. Haffter, J. Brandani, B. Therrien, E. Gregoire, M. Bergström, F. Bielser and D. Resch who assisted with laboratory work.

Author contributions

The project was conceived by T.J.B., H.P. and T.J.K. Sample collection was performed by the Vanishing Glaciers Field Team. Laboratory work was performed by T.J.K., H.P., N.D., M. Styllas and members of the Vanishing Glaciers Field Team. Data analyses were performed by T.J.K., H.P. and M.B., with further analyses and interpretation by T.J.B, R.L.S. and G.Y.-D. The first draft of the manuscript was written by T.J.B. and T.J.K., with further editing and input from all authors.

Funding

Open access funding provided by EPFL Lausanne

Competing interests

The authors declare no competing interests.

Additional information

Extended data is available for this paper at https://doi.org/10.1038/s41561-024-01393-6.

Correspondence and requests for materials should be addressed to Tyler J. Kohler or Tom J. Battin.

Peer review information *Nature Geoscience* thanks Sophie Cauvy-Fraunié, Jonathan Benstead, Kyra St. Pierre and the other, anonymous, reviewer(s) for their contribution to the peer review of this work. Primary Handling Editor: Xujia Jiang, in collaboration with the *Nature Geoscience* team.

https://doi.org/10.1038/s41561-024-01393-6

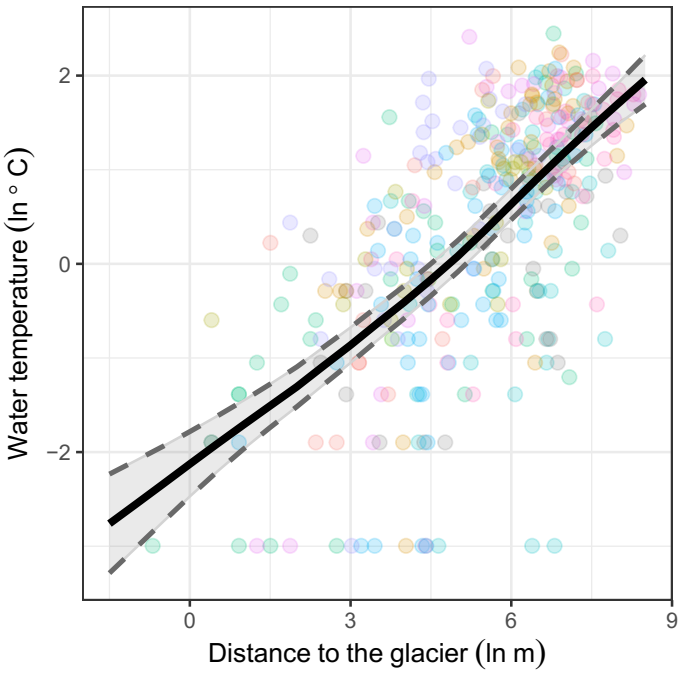

Extended Data Fig. 1 | Water temperature increases with greater distance from the glacier in glacier-fed streams. Generalized additive mixed models (GAMMs) accounting for the spatial structure of the data, and combined with a Bayes factor analysis to select relevant variables, revealed that streamwater temperature of GFSs increases with increasing distance from the respective source glacier. Shown are the response curves with 95% prediction intervals; full GAMM results are provided in Extended Data Table 1. Colors represent the corresponding mountain ranges provided in the map (Fig. 1a).

https://doi.org/10.1038/s41561-024-01393-6

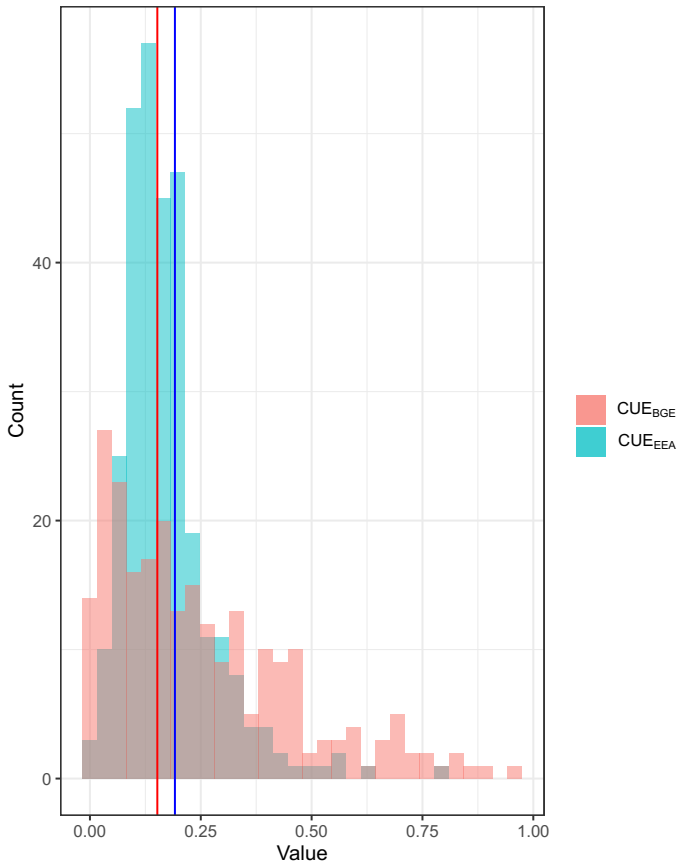

Extended Data Fig. 2 | Carbon use efficiency (CUE) values obtained through modeling are comparable to those obtained through manual measurements. Shown are the distributions of CUE calculated using the activity of extracellular enzymes (CUE_{EEA}) and CUE calculated from measurements of bacterial carbon production and respiration (CUE_{BGE}). Median values for both estimates are shown as vertical lines (CUE_{EEA} = 0.15, CUE_{BGE} = 0.23). While the median estimates agree well and align with literature expectations, CUE_{BGE} varies more than CUE_{EEA} probably because of compound effects of variation in the measurements of bacterial carbon production and community respiration.

https://doi.org/10.1038/s41561-024-01393-6

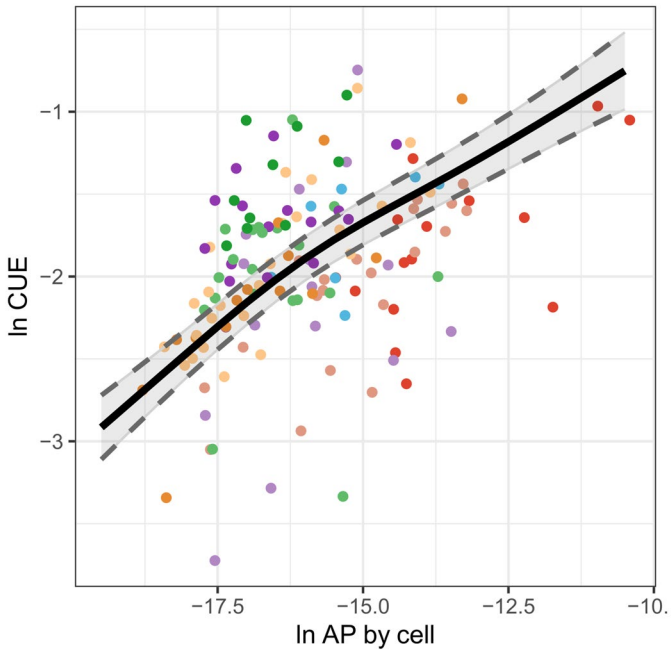

Extended Data Fig. 3 | Carbon use efficiency (CUE) increases with increasing phosphatase (AP) activity in glacier-fed streams. General additive mixed models (GAMM) accounting for the spatial structure of data, and combined with a Bayes factor analysis to select relevant variables, indicated that CUE is significantly and positively related to cell-specific AP activity ($n = 142$, $F = 22.247$, $p < 0.001$). Shown are the response curves with 95% prediction intervals. No adjustments for multiple comparisons were made, and reported p-values are two sided; full GAMM results are provided in Extended Data Table 1. Colors represent the corresponding mountain ranges provided in the map (Fig. 1a).

https://doi.org/10.1038/s41561-024-01393-6

Extended Data Table 1 | Full output for all generalized additive mixed models (GAMMs)

Tested variable	Parametric coefficients					Approximate significance of smooth terms:							
	Term	Estimate	Std. Error	t-value	Pr(>|t|)	Term	edf	Ref.df	F	p-value	Adj. R^2	Scale est.	n
turbidity	(Intercept)	3.78322	0.09004	42.02	<2e-16	s(latitude,longitude)	17.938	49	3.642	<2e-16	0.523	1.5664	332
						te(gl_area)	1.196	4	9.45	<2e-16			
water temperature	(Intercept)	0.39013	0.05537	7.046	1.10E-11	s(latitude,longitude)	5.358	49	0.25	0.0107	0.496	0.84962	338
						te(gl_area,gl_dist)	6.551	24	13.62	<2e-16			
DOC	(Intercept)	5.14796	0.03235	159.1	<2e-16	s(latitude,longitude)	21.12	49	2.509	<2e-16	0.423	0.17686	169
SRP	(Intercept)	1.14538	0.04678	24.48	<2e-16	s(latitude,longitude)	39.759	49	9.261	<2e-16	0.706	0.46684	301
						te(gl_area)	0.762	4	0.719	0.0402			
DIN	(Intercept)	4.4812	0.0387	115.8	<2e-16	s(latitude,longitude)	23.9	49	11.79	<2e-16	0.769	0.27486	309
chlorophyll-*a*	(Intercept)	-5.8846	0.1562	-37.66	<2e-16	s(latitude,longitude)	27.836	49	5.186	<2e-16	0.616	5.1172	302
						te(turbidity,DIN)	4.333	24	1.909	<2e-16			
$TER_{C:N}$	(Intercept)	4.844133	0.004401	1101	<2e-16	s(latitude,longitude)	8.891	49	0.726	9.94E-06	0.13	0.004678	261
$TER_{C:P}$	(Intercept)	5.26786	0.05883	89.54	<2e-16	s(latitude,longitude)	19.254	49	1.86	<2e-16	0.382	0.68872	261
						te(chla)	1.174	4	7.034	<2e-16			
CUE	(Intercept)	-1.8774	0.02903	-64.68	<2e-16	s(latitude,longitude)	19.665	49	1.855	<2e-16	0.378	0.16671	261
						te(chla)	1.161	4	6.54	<2e-16			
CUE	(Intercept)	-1.91974	0.02487	-77.18	<2e-16	s(latitude,longitude)	28.779	49	4.425	<2e-16	0.682	0.087861	142
						te(AP_cell)	1.988	4	22.247	<2e-16			
Respiration	(Intercept)	-9.95077	0.18419	-54.025	<2e-16	s(chla)	2.416	4	7.214	1.27E-06	0.133	0.86105	243
	rel_temp	-0.03071	0.15875	-0.193	0.847								
BCP	(Intercept)	3.855	0.1755	21.972	<2e-16	s(chla)	1.468	4	18.75	<2e-16	0.29	1.0999	297
	rel_temp	-0.6226	0.1453	-4.285	2.48E-05								
CUE	(Intercept)	-1.83875	0.09317	-19.735	<2e-16	s(chla)	1.098	4	5.034	6.78E-06	0.0661	0.29146	299
	rel_temp	-0.06688	0.07854	-0.851	0.395								
cell-specific AP	(Intercept)	-16.0534	0.2315	-69.356	<2e-16	s(chla)	2.633	4	8.843	<2e-16	0.107	2.206	301
	rel_temp	0.1188	0.1875	0.633	0.527								

Abbreviations used here include: DOC = dissolved organic carbon, SRP = soluble reactive phosphorus, DIN = dissolved inorganic nitrogen, TER = threshold elemental ratio, CUE = carbon use efficiency, BCP = bacterial production, AP = alkaline phosphatase, rel_temp = inverse relative water temperature, gl_area = glacier area, gl_dist = distance to glacier, chla = chlorophyll-*a*, AP_cell = cell-specific AP. No adjustments for multiple comparisons were made, and reported p-values are two sided. See Extended Data Table 3 for more details on model structure.

https://doi.org/10.1038/s41561-024-01393-6

Extended Data Table 2 | Summary statistics for key measured parameters

Parameter	q25	median	q75	median difference (upper vs. lower reach)	p-value
glacier index	0.002	0.005	0.021	0.016	2.51E-29
glacier area (km^2)	0.64	1.99	6.43	0	1.67E-12
distance to glacier (m)	72.0	318.5	881.5	-515.0	2.14E-29
glacier coverage (%)	0.38	0.53	0.66	0.05	1.82E-26
turbidity (NTU)	12.9	48.4	181.1	0.9	0.545
conductivity ($\mu S\ cm^{-1}$)	12.6	54.1	106.3	0.2	0.074
water temperature (°C)	0.6	2.0	4.0	-1.7	4.24E-21
respiration (ng O_2 g^{-1} DM hr^{-1})	26.33	42.60	75.20	8.96	0.081
BCP (ng C g^{-1} DM hr^{-1})	5.46	12.49	30.07	-3.27	8.08E-06
chlorophyll-*a* (ng chla g^{-1} DM)	0.69	5.56	27.21	-0.23	0.002
DOC (ppb)	103.3	150.7	239.4	NA	NA
DIN (ppb)	32.3	95.3	196.4	7.3	1.73E-07
SRP (ppb)	1.3	2.5	6.5	-0.1	0.339
streamwater N:P	12.13	72.12	274.58	2.41	0.003
streamwater C:N	0.82	1.81	5.36	NA	NA
streamwater C:P	43.99	134.44	315.22	NA	NA
CUE	0.110	0.151	0.205	-0.011	0.030
$TER_{C:N}$	93.9	96.2	101.6	-0.056	0.876
$TER_{C:P}$	95.8	179.9	346.7	12.4	0.030
LAP (nmol h^{-1} g^{-1} DM)	0.655	1.907	6.390	-0.169	0.005
BG (nmol h^{-1} g^{-1} DM)	0.036	0.127	0.438	-0.014	0.018
AG (nmol h^{-1} g^{-1} DM)	0.008	0.026	0.114	-0.005	0.000
AP (nmol h^{-1} g^{-1} DM)	0.172	0.660	2.488	-0.079	0.005
NAG (nmol h^{-1} g^{-1} DM)	0.010	0.042	0.153	-0.008	0.002

For each variable, we report 0.25, 0.50, and 0.75 quantiles (q25, median, q75), the median difference between upper and lower reaches, and two-sided p-values from Wilcoxon tests comparing upper and lower reaches. Streamwater C:N:P designate the molar ratios of inorganic dissolved nutrients in streamwater, and LAP, BG, AG, AP, and NAG are enzymatic activities (leucine aminopeptidase, β-1,4-glucosidase, α-1,4-glucosidase, alkaline phosphatase, and β-1,4-N-acetylglucosaminidase, respectively). All other abbreviations are given in the caption of Extended Data Table 1. The formula for the glacier index is given in refs. 50,53.

https://doi.org/10.1038/s41561-024-01393-6

Extended Data Table 3 | Structure of individual generalized additive mixed models (GAMMs)

Dependent variable(s)	Independent variable(s)	Autocorrelation	Spatial spline structure
temperature, turbidity, DOC, DIN, and SRP	all combinations of distance from glacier, % glacier coverage, and glacier area in a tensor, best combination picked based on a Bayes factor analysis	corCAR1(form = ~1|GFS)	latitude and longitude, bs = 'sos', m=1, k=-1
chlorophyll-*a*	all combinations of turbidity, water temperature, SRP, and DIN in a tensor, best combination picked based on a Bayes factor analysis	corCAR1(form = ~1|GFS)	latitude and longitude, bs = 'sos', m=1, k=-1
CUE, $TER_{C:N}$, and $TER_{C:P}$	all combinations of water temperature, chlorophyll-*a*, and streamwater N:P in a tensor, best combination picked based on a Bayes factor analysis	corCAR1(form = ~1|GFS)	latitude and longitude, bs = 'sos', m=1, k=-1
CUE	AP per cell as a spline	corCAR1(form = ~1|GFS)	latitude and longitude, bs = 'sos', m=1, k=-1
respiration, BCP, CUE, AP per cell	Inverse relative water temperature as a linear effect, accounting for chlorophyll-*a* with a spline	corCAR1(form = ~1|GFS)	NA

Here we report the structure of each GAMM tested, including dependent variable(s), independent variable(s), and the spatial spline structure. For all, family = gaussian and link function = identity.